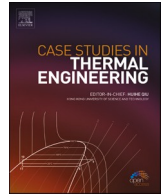




ELSEVIER

Contents lists available at ScienceDirect

## Case Studies in Thermal Engineering

journal homepage: [www.elsevier.com/locate/csite](http://www.elsevier.com/locate/csite)

# Development of laminar burning velocity measurement system in premixed flames with hydrogen-content syngas or strong oxidizer conditions in a slot burner

Yueh-Heng Li <sup>a,b,\*</sup>, Jin-Wei Liang <sup>a,c</sup>, Hung-Ju Lin <sup>a</sup>

<sup>a</sup> Department of Aeronautics and Astronautics, National Cheng Kung University, Tainan, 701, Taiwan

<sup>b</sup> International Bachelor Degree Program on Energy, National Cheng Kung University, Tainan, 701, Taiwan

<sup>c</sup> Industrial Upgrading Service Department, Metal Industries Research & Development Center, Kaohsiung, 811, Taiwan

## ARTICLE INFO

## Keywords:

Laminar burning velocity  
Schlieren measurement  
Multiple fuels  
Nitrous oxide

## ABSTRACT

This study presents the experimental determination of laminar burning velocity for critical premixed flames with multiple fuels or strong oxidizers. Experiments were conducted with a slot burner under methane/air, methane/nitrous oxide, and syngas (CH<sub>4</sub>/CO/H<sub>2</sub>)/air premixed flames conditions with varying equivalence ratios from 0.8 to 1.4. With the flame surface area determined from the Schlieren measurement system and stretch effect corrected by Markstein length, unstretched laminar burning velocity can be garnered according to the conservation of mass. First, the experimental results of methane/air premixed flame velocities were validated by comparing with one-dimensional unstretched burning velocities through numerical simulations with GRI 3.0 mechanism. The experimental results in the equivalence ratio ranging from 0.85 to 1.2 demonstrated errors less than 3.8%. Then, the validated burning velocity measuring techniques were implemented under methane/nitrous oxide and syngas/air premixed flame conditions. Finally, appropriate chemical mechanisms, such as USM or UGM, can be validated for the numerical simulation of critical premixed flames via this proposed laminar burning velocity measuring technique.

## Nomenclature

$A$	Flame area, cm <sup>2</sup>
$A_1$	Mixture strength
$D$	Mass diffusivity, cm <sup>2</sup> /s
$D_{i,mix}$	Mixture-averaged mass diffusivity, cm <sup>2</sup> /s
$E_a$	Activation energy, J/mol
$K$	Stretch rate, 1/s
$k$	Cubic law coefficient
$L$	Characteristic length, m
$Le$	Lewis number
$Le_{f/oxidizer}$	Combination of $Le$ associated to the fuel and oxidizer

\* Corresponding author. Department of Aeronautics and Astronautics, National Cheng Kung University, Tainan, 701, Taiwan.  
E-mail address: [yueheng@mail.ncku.edu.tw](mailto:yueheng@mail.ncku.edu.tw) (Y.-H. Li).

<https://doi.org/10.1016/j.csite.2022.102162>

Received 11 November 2021; Received in revised form 26 May 2022; Accepted 28 May 2022

Available online 31 May 2022

2214-157X/© 2022 The Authors. Published by Elsevier Ltd. This is an open access article under the CC BY license (<http://creativecommons.org/licenses/by/4.0/>).

$L_M$	Markstein length
$M$	Dynamic viscosity, kg/m • s
$\dot{m}$	Mass flow rate, g/s
$Pe_{cl}$	Critical Péclet number
$Pe_{pr}$	Heat transfer Péclet number
$Pe_{sc}$	Mass transfer Péclet number
$Pr$	Prandtl number
$P_0$	Initial pressure, Bar
$P_{max}$	$P_0 + \Delta P_{max}$ , Bar
$\Delta P_{max}$	Variation of max pressure, Bar
$R$	Universal gas constant, J/K mol
$R_B$	Light radius, cm
$Re$	Reynolds number
$R_s$	The radius of the spherical vessel, m
$Sc$	Schmidt number
$S_L^0$	Unstretched laminar burning velocity, cm/s
$S_u$	Unburned gas velocity, cm/s
$T_b$	Adiabatic flame temperature, K
$T_u$	Unburned gas temperature, K
$u$	Flow velocity, m/s
$\nu$	Kinematic viscosity, m <sup>2</sup> /s
$X$	Molar fraction
$Y_{i,mix}$	Mass fraction
$Ze$	Zeldovich number
$\alpha$	Thermal diffusivity, cm <sup>2</sup> /s
$\alpha^\circ$	Expansion factor
$\beta$	The complementary angle of half flame tip angle
$\gamma$	Density ratio
$\delta_L^\circ$	Thermal flame thickness, cm
$\eta_1$	First correction factor
$\eta_2$	Second correction factor
$\rho$	Density of the fluid, kg/m <sup>3</sup>
$\rho_L$	Density of the burned mixture, g/cm <sup>3</sup>
$\rho_u$	Density of the unburned mixture, g/cm <sup>3</sup>
$\varphi$	Equivalence ratio

## 1. Introduction

The purpose of studying the combustion process is to understand its chemical, thermodynamic, and fluid properties. Laminar burning velocity is an important parameter that contains the effect of reactivity, diffusivity, and exothermicity in any premixed flame. However, there are several difficulties in determining unstretched laminar burning velocity ( $S_L^0$ ) in experiments. In the real combustion process, a flame is subjected to boundary effects and unsteady species diffusion, which lead to flame stretch. The flame stretch rate, which was derived by Matalon [1], can be expressed  $K = \frac{1}{A} \frac{dA}{dt}$ . Here,  $K$  is the stretch rate (1/s) and  $A$  is the flame surface area (m<sup>2</sup>). Flame stretch can be considered the rate of change in the flame area. Accordingly, experimental measurements of laminar burning velocity have been conducted on stretched flames for decades because a stable, unstretched, and adiabatic combustion is difficult to achieve. Most studies converted stretched to unstretched laminar burning velocity by compensating the velocity loss or gain based on some critical parameters that are related to combustion.

In addition, some dimensionless parameters are crucial in determining the laminar burning velocity of hydrocarbon fuels. The Lewis number ( $Le$ ) refers to the ratio of the thermal diffusivity ( $\alpha$ ) to the mass diffusivity ( $D$ ) of the deficient reactant, that is, the fuel for fuel-lean mixtures or oxidizer for fuel-rich mixtures [2]. In addition, thermal diffusion and mass diffusion also affect the stretch rate. For instance, a negative stretch rate with high  $\alpha$  and low  $D$  values results in higher laminar burning velocity. Consequently, the Lewis number plays an essential part in fluid analysis, and it has been widely studied in combustion research [2–4]. The flame is stable when  $Le > 1$ , and less sensitive to the flame stretch. On the contrary, the wrinkles of the flame grow with a decreasing  $Le$  value [5–7]. Péclet number ( $Pe$ ) is a dimensionless parameter that refers to the ratio between the advection rate of a physical quantity by a flow and the diffusion rate of the same quantity by a gradient. It can also be defined as  $Pe_{sc}$  and  $Pe_{pr}$  in mass transfer and heat transfer, respectively.  $Pe_{sc}$  and  $Pe_{pr}$  can be expressed as  $Pe_{sc} = ReSc$  and  $Pe_{pr} = RePr$ , respectively. In several studies on combustion,  $Pe_{pr}$  has been proved to have the ability to indicate flame stability [8–11]. Bradley et al. [10,11] analyzed the relationship between  $Pe_{pr}$  and flame stability in a spherical gas explosion. The cellular structure appears when  $Pe_{pr} > Pe_{cl}$  (critical  $Pe$  number), leading to flame instability. Makhviladze

et al. [12] analyzed the quenching and flammability limits of the propagation flame in the channel. It is concluded that flammability can be characterized by  $Pe_{cl}$ .

Different measurement systems of laminar burning velocity have been extensively developed. Li et al. [42] compared measured and simulated burning velocities of oxy-methane combustion in  $N_2$ ,  $CO_2$ ,  $H_2O$ , and fluegas dilution. In the meantime, Mazas et al. [13] measured the laminar burning velocity of methane/air premixed flame by adding water vapor. They provided a calculation procedure that includes the Zeldovich number, Lewis number, flame cone area, and Markstein length [13,42]. To determine the flame cone area, they employed Schlieren imaging in the Z-arrangement setup and vertical knife-edge cutoff to capture the photo of the flame cone on a conical burner. The flame cone boundaries were acquired by applying Sobel edge detection. One-dimensional, freely propagating, unstretched, and adiabatic numerical simulations of methane/air have been conducted in PREMIX code with the GRI 3.0 mechanism. Mazas et al. [13] compared the experimental laminar flame speed from different literature with the numerical results under the variation of equivalence ratios. However, the stretched and curvature effect on the conical flame is complicated. The flame cone area determined through Schlieren measurement is affected by line-of-sight integration in the conical burner. Therefore, the experimental laminar burning velocities are lower than the numerical simulation results because of heat losses at the burner rim. Razus et al. [14] calculated the experimental laminar burning velocity of nitrogen-diluted methane/nitrous oxide mixture using the time-dependent pressure equation with the cubic law coefficient. For numerical data, one-dimensional and isobaric numerical simulations were conducted in COSILAB with GRI 3.0. They concluded that the GRI 3.0 underestimates the laminar burning velocity and suggested that several rate constants be replaced according to their sensitivity analysis. Because the experimental data calculated by Razus et al. [14] are stretched values, the stretched data are slightly higher than the unstretched data acquired from the flat flame burner reported by Powell et al. [15].

Selle et al. [16] proposed a calculation method, Eq. (1), using two correction factors for converting stretched to unstretched laminar burning velocity derived from simulations and experimental results.

$$S_L^0 = S_L \eta_1 \eta_2 \quad (1)$$

The first correction factor,  $\eta_1$ , considers stretch, curvature effect, and heat loss, whereas the second correction factor,  $\eta_2$ , rectifies the velocity acceleration in the center of the slot burner due to the boundary effect. Additionally,  $\eta_1$  is derived from the comparison between stretched and unstretched ratios from numerical results. However,  $\eta_2$  is determined by the conversion of the two-dimensional (2D) bulk velocity profile from the mean velocity of the unburned gas by experiments or numerical simulations. The laminar burning velocities of methane/air mixture premixed flame were measured using slot burners with the equivalence ratio ranging from 0.8 to 1.2. The principle of acquiring stretched laminar burning velocity differs from that of Mazas et al. [13]. However, the calculation method is only suitable for the mixture's Lewis number near unity. For  $H_2$  mixture cases,  $\eta_1$  is no longer valid because of the oscillated value. Chong et al. [17] reported a measurement system for the laminar burning velocities of Jet-A1, diesel, palm methyl esters (PME), and blends of PME with diesel and Jet-A1 fuels using particle image velocimetry (PIV) on the stagnation flame. The strain rate was determined by the ratio of axial velocity to radial velocity gradient. Additionally, unstretched laminar burning velocity was calculated by applying linear extrapolation of unburned gas velocity along with the axial and radial directions. Wang et al. [18] measured the laminar burning velocity of  $CH_4/O_2/N_2$  and  $CH_4/O_2/CO_2$  using the heat flux method. They conducted numerical simulations with GRI 3.0 and HP-Mech mechanism using Chemkin Pro. One great advantage of the heat flux method is that it can compensate for the heat losses at the boundary of the burner. The unstretched laminar burning velocity can be determined directly from the unburned gas velocity by achieving zero net heat flux at the burner plate. However, the unburned gas velocity can be affected by thermocouples attached to the burner plate. Nevertheless, additional heaters are required to compensate for the heat losses.

$CH_4$ /air mixtures are widely used for testing burners and validating measurement systems [16,19]. However, the combustion of  $CH_4$  with a strong oxidizer, e.g.,  $N_2O$  [20,21], or syngas ( $H_2$ ,  $CH_4$ , and  $CO$ ) [22–24] with air, is prevailing to utilize in industrial sectors. Compared with hydrocarbon/air combustion, replacing air with  $N_2O$  as an oxidizer can significantly increase the oxidation process [25,26]. The heat release of fuel/ $N_2O$  combustion is higher than that of fuel/air mixtures because of the  $N_2O$  decomposition accompanying enormous exothermicity [21,27]. Konnov et al. [28] presented the experimental measurements of the adiabatic burning velocity in neat and  $NO$  formation in oxygen/methane/argon flames doped with small amounts of  $N_2O$ . Powell et al. [15] compared the experimental laminar burning velocities of  $H_2$ ,  $CH_4$ ,  $C_2H_2$ , and  $C_3H_8/N_2O$  flames with numerical results based on different mechanisms. They reported that current mechanisms always underpredict fuel/ $N_2O$  characteristics.

Syngas compositions are diverse, and most of the combustion usually includes  $CH_4$ ,  $CO$ , and  $H_2$ . Scholte et al. [29] measured the laminar burning velocity of  $H_2$ ,  $CH_4$ , and  $CO$ /air syngas. They reported that the velocity increases with the ratio of  $H_2$  in fuel composition. Cherian et al. [30] concluded that the ratio of  $H_2$  dominates the value of laminar burning velocity among other fuels ( $CO$  and  $CH_4$ ).

Most measurement methods can acquire stretched laminar burning velocity easily. However, the value of the unstretched laminar burning velocity is required to validate the experimental results with simulations and other studies. There are two critical elements for the conversion from stretched to unstretched value. One element is flame stretch, and the other element is the Markstein length,  $L$ . The Markstein length is given as follows:

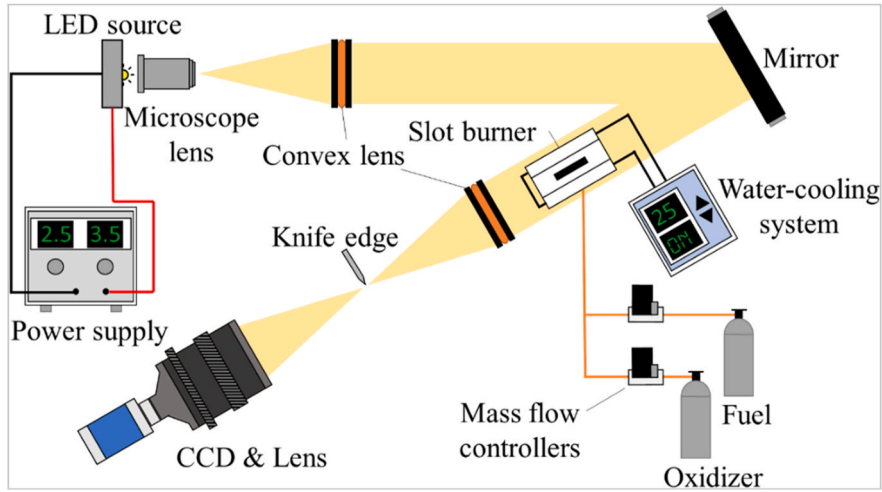


Fig. 1. Schlieren imaging system.

$$L = \delta_L^* \left[ \frac{1}{\gamma} \ln \left( \frac{1}{1-\gamma} \right) + \frac{Ze(Le-1)(1-\gamma)}{2\gamma} \int_0^{\frac{r}{r_f}} \frac{\ln(1+x)}{x} \right] \quad (2)$$

Here,  $\gamma = \frac{T_f - T_u}{T_f}$  is the heat release parameter;  $T_f$  is the adiabatic flame temperature (K); and  $T_u$  is the unburned gas temperature (K). Additionally,  $Ze$  denotes the Zeldovich number, which is the nondimensionalized activation energy, expressed by Eq. (3);  $Le$  is the Lewis number; and  $\delta_L^*$  is the thermal flame thickness (m). The magnitude of the Markstein length indicates the effect of curvature on laminar burning velocity.

$$Ze = \frac{E_a}{RT_b} \frac{T_b - T_u}{T_b} \quad (3)$$

Another approach for converting the stretched flame is to apply the correction factor,  $\eta_1$ , for stretch laminar burning velocity [16]. However,  $\eta_1$  depends on the mixture's Lewis number. Therefore, establishing a detailed method to examine combustion characteristics is essential. This study provides a measurement system combining stretch, the Lewis number ( $Le$ ), the Zeldovich number ( $Ze$ ), the calculation in the study of Mazas et al. [13], and the velocity distribution correction factor  $\eta_2$  in the study of Selle et al. [16]. This study developed a laminar burning velocity measuring system with multifuel or strong oxidizer premixed flames. Low Lewis number mixtures and high temperature combustion cases are included in this study to expand the application of this measurement system.

## 2. Experiment and numerical simulation setup

### 2.1. Schlieren imaging system and slot combustor

In a combustion process, the determination of flame front position is essential. The visible, Schlieren, and shadowgraph edges represent different positions of the flame front [30]. The visible edge of the flame cone is located after the initial temperature rise and cannot represent the position of the flame front. Shadowgraph edge can be affected by the distance between the object and the final image position. Nevertheless, its inner edge is located before the preheat zone. Rallis et al. [31] concluded that Schlieren imaging could indicate the start of the preheat zone and cover most of the flame thickness.

Before conducting the Schlieren imaging on premixed flames, it is necessary to determine the suitable light blockage area percentage. Bunjong et al. [32] found that the contrast level of the image increases with the blockage percentage. It means that the density variation can be intensified with a higher blockage percentage. However, a high blockage area percentage may lead to insufficient light intensity, resulting in low image quality. The present study fixed the blockage area percentage to 50% for achieving sufficient intensity and high image quality.

Fig. 1 shows a schematic of the experimental setup. The Schlieren imaging system consists of convex lenses, LED point light source, adjustable power supply, knife-edge, and CCD. First, the LED light source is activated by the power supply under working voltage and ampere. Second, the first convex lens creates a parallel light testing area from the LED light source at the focal point. Third, a plane mirror is installed at the end of the workstation to extend and turn the parallel light. Fourth, the second convex lens focuses the light to a small point to perform knife-edge cutoff at the focal point. Eventually, the flame images are taken by Pixelfly USB CCD equipped with a Nikkor lens (AF Micro-Nikkor 60 mm f/2.8D).

Two convex lenses with the same diameter, 0.05 cm, are installed on an optical mount. The optical mount is equipped with a level

adjustment device. The focal length of both lenses is 400 mm. White light LED operates under 3.2–3.5 V with 1.9–2.5 A. Twintex TP-3020 can provide one channel 0–30 V output voltage and 0–20 A output ampere in DC current. A sharp knife-edge is installed on a turning mount with a horizontal cutoff direction. PCO pixelfly CCD has a maximum resolution of  $1392 \times 1040$  pixels with 14-bit depth and 4000:1 dynamic range. All adjustments can be controlled using PCO camware.

Fuel and oxidizer flow rates are controlled by mass flow controllers (Model 5850E, Brooks Instrument, US) and calibrated by a primary flow calibrator (Definder 220, Bios, US). The correlation coefficient of setting values and actual values is 0.9999. The fuel and oxidizer are premixed in the bottom of the slot burner, which is filled with stainless steel beads. Then, the gas travels through a high-density mesh nozzle section to obtain laminar flow. The equivalence ratio of the flame in the experiment ranges from 0.8 to 1.4. The dimension of the slot burner is  $200 \text{ mm} \times 110 \text{ mm} \times 14 \text{ mm}$  (without a water-cooling segment). The burner is designed in a rectangular exit ( $4 \text{ mm} \times 40 \text{ mm}$ ) to avoid the deviation caused by line integration [33] of the conical burner. It is recommended that the ratio of the long side to the short side is 10:1 [34]. A detailed structure of the slot burner is displayed in **Figure a** in the supplementary material. The slot burner contains three parts: gases are mixed in the bottom section, and the mesh and nozzle sections are used to generate a flat velocity profile at the exit. An additional water-cooling segment (flow rate:  $0.00012 \text{ m}^3/\text{s}$ ) is installed on both sides of the slot burner to avoid thermal gradient during the experiment. All mixtures are presented in **Tables a-e** in the supplementary material.

## 2.2. Calculation of laminar burning velocity

The area-weighted average flame speed can be calculated from the mass flow rate based on the conservation of mass between the burner exit and flame front (Eq. (4)).

$$\dot{m} = \rho_u S_u A \quad (4)$$

Here,  $\dot{m}$  is the mass flow rate of the unburned gas,  $\rho_u$  the unburned gas density,  $S_u$  is the unburned gas speed, and  $A$  is the flame surface area (flame length in 2D).  $S_u$  can be considered the stretched laminar burning velocity  $S_L$ . The flame surface area (flame length in 2D) can be obtained by analyzing Schlieren images with sober edge detection or asymptote fitting. The Schlieren image is averaged over 100 images in 14-bit depth to eliminate the uncertainties of mass flow controllers and CCD. The flame measurement is conducted at the central part of the slot burner (indicated by white rectangular in **Figure b** in the supplementary material), where the flame front is flat, and the stretch effect on the edge is not included. The curvature effects on the flame tip and base are neglected during the calculation process.

The Schlieren imaging cuts out unwanted chemical luminous and preserves a more precise flame cone area. However, there is a white to the black gradient at the flame front boundary because the acquired images' gray level value ranges from 0 to 16,383. Therefore, additional post-processing coded in Matlab must be applied to extract a clearer flame front boundary for analysis.

The Matlab code for image post-processing can convert gray-level images to binary images by setting the threshold of the gray level. By applying asymptote fitting on the binary image of the inner flame front between burned and unburned gas, the flame length, and angle of the flame cone can be attained. The actual dimension of the flame in the Schlieren image is calibrated in every experiment.

To convert a stretched velocity to unstretched velocity, a compensation for calculating unstretched laminar burning velocity in the study of Mazas et al. [13] is given by

$$S_L^0 = S_L + LK. \quad (5)$$

Here,  $K$  is the stretch rate, and  $L$  is the Markstein length, which can be decomposed as follows [13]:

$$L = \frac{Ze}{2} \left( 1 - \frac{1}{Le} \right) \alpha^\circ \delta_L^\circ. \quad (6)$$

Here,  $\alpha^\circ = 1 + \log_e \left[ \frac{T_u}{T_b} + \left( 1 - \frac{T_u}{T_b} \right) e^{-1} \right]$  is the expansion factor;  $T_b$  is the adiabatic flame temperature (K); and  $T_u$  is the unburned gas temperature (K). In the study of Selle et al. [16], the velocity correction factor  $\eta_2 = 1.067$  is calculated by numerical simulation of flow field from Ref. [34] for a slot burner with the aspect ratio of 10:1. Combining  $\eta_2$  and the Markstein length can lead to a new equation for calculating unstretched laminar burning velocities in slot burner premixed combustions, which is given by

$$S_L^0 = S_L \eta_2 + LK \quad (7)$$

The experimental and calculated values are as follows:

- I. Stretched laminar burning velocity  $S_L$
- II. Thermal flame thickness  $\delta_L^\circ$
- III. Stretch rate  $K$

The numerical simulation values are as follows:

- I. Zeldovich number  $Ze$
- II. Expansion factor  $\alpha^\circ$
- III. Lewis number  $Le$
- IV. Velocity correction factor  $\eta_2$

The calculation of  $Ze$  requires the activation energy ( $E_a$ ) of the mixtures (Detail calculation process is displayed to supplementary

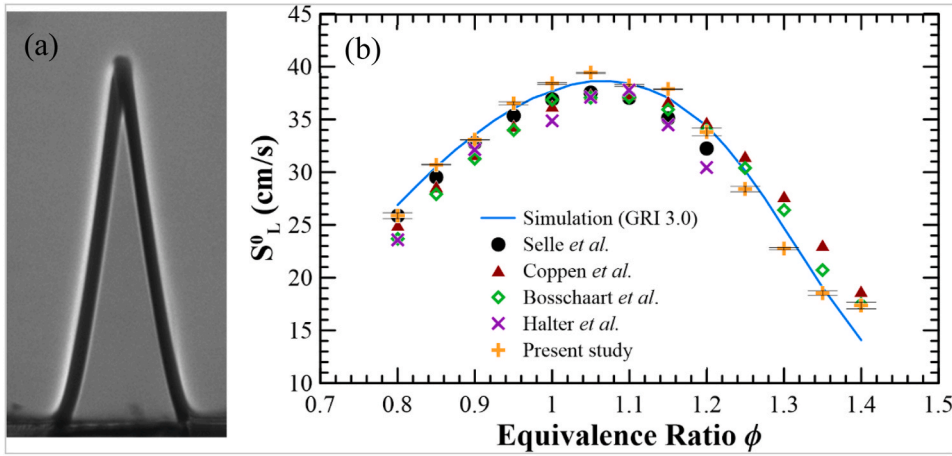


Fig. 2. (a) 50% blockage Schlieren imaging photo with CH<sub>4</sub>/air premixed flame at  $\phi = 1.0$ , (b) numerical and experimental laminar burning velocity of CH<sub>4</sub>/air mixtures from  $\phi = 0.8$  to 1.4.

material).  $Ze$  can be calculated by extrapolating the natural logarithm of mixture mass flow rate and the reciprocal adiabatic flame temperature. The coefficient in the fitting line equation represents  $\frac{E_a}{2R}$ , where  $R$  is the gas constant. Eq. (7) solves the problem that the numerical correction factor  $\eta_1$  for the flame stretch in the study of Selle et al. [16] cannot apply for nonunity,  $Le$ , and corrects the boundary effect on velocity profile in the slot burner.

Regarding the determination of Lewis number, Lapalme et al. [2] proposed an effective  $Le$  calculation method. Most fuel/air mixtures' mass diffusivity ( $D$ ) is calculated in binary  $D_{ij}$ . Here,  $i$  refers to fuel and  $j$  represents N<sub>2</sub> because it takes the most percentage in the fuel/air mixtures. However, the aforementioned calculation is unsuitable for multifuel or H<sub>2</sub> mixture cases. Eq. (8) presents an alternative calculation for  $D$ ,

$$D_{i,mix} = (1 - Y_{i,mix}) \left( \sum_{s=1, s \neq i}^N \frac{X_s}{D_{is}} \right)^{-1}, \quad (8)$$

where  $Y$  is the mass fraction,  $X$  is the molar fraction, and  $s$  is the species in the mixture. The overall calculation of an effective  $Le$  follows that of the study of Lapalme et al. [2]. First, mixture-averaged mass diffusivity  $D_{i,mix}$  and  $\alpha_i$  for each fuel and oxidizer are calculated. Second, mix  $Le_i$  by volume fraction to derive  $Le_{fuel}$  and  $Le_{oxidizer}$ . Finally, combining  $Le_{fuel}$  and  $Le_{oxidizer}$  by considering the excessive and deficient reactants with mixture strength ( $A_1$ , Eq. (9)) leads to  $Le_{f/oxidizer}$ , Eq. (10).

$$A_1 = 1 + Ze(\Omega - 1), \Omega = \frac{1}{\phi} \text{ for } \phi \leq 1, \Omega = \phi \text{ for } \phi > 1 \quad (9)$$

$$Le_{f/oxidizer} = 1 + \frac{(Le_{exc} - 1) + (Le_{def} - 1)A_1}{1 + A_1}. \quad (10)$$

In the calculation of mixture strength,  $\Omega$  is defined relative to the equivalence ratio,  $\phi$ .  $Le_{exc}$  and  $Le_{def}$  in Eq. (10) represent the excessive and deficient  $Le$  of the reactant, respectively. All properties of elements are taken from the databases of the National Institute of Standards and Technology.

### 2.3. Numerical simulation

All numerical simulations were conducted in ANSYS Chemkin Pro. The adiabatic flame temperature is calculated using the equilibrium reactor model. This model helps users to determine a mixture's chemical state in an equilibrium state. Gases and condensed phases are assumed to be ideal solutions in the equilibrium program. An initial temperature guess is required to determine the burned mixture solution. All adiabatic flame temperatures are completed with GRI 3.0 even for CH<sub>4</sub>/N<sub>2</sub>O cases because the value difference between mechanisms is minor.

For calculating unstretched laminar burning velocities, a series of one-dimensional, premixed, and free propagating numerical simulations (premixed flame model) are completed with the GRI 3.0 mechanism for CH<sub>4</sub>/air and syngas, USM and UGM mechanism [35] for CH<sub>4</sub>/N<sub>2</sub>O. The Premixed Flame Model can simulate a freely propagating flame, where the reference point is a fixed position on the flame. In this coordinate system, the flame speed is defined as the inlet velocity that allows the flame to stay in a fixed location, which is an eigenvalue of the solution method. The GRI 3.0 mechanism consists of 53 species and 325 elementary chemical reactions. It is commonly used for C1–C3 chemical reactions, especially for CH<sub>4</sub> mixtures. The simulation results of CH<sub>4</sub> have been validated by several studies [13,36].

USM and UGM mechanisms were modified from UG and US mechanisms and proposed by Wang et al. [35]. UG mechanism is

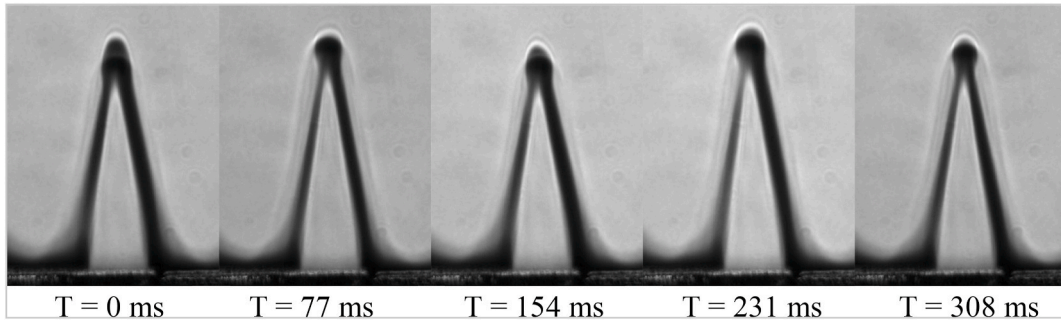


Fig. 3. Schlieren images of CH<sub>4</sub>/air premixed flame at  $\phi = 1.4$ .

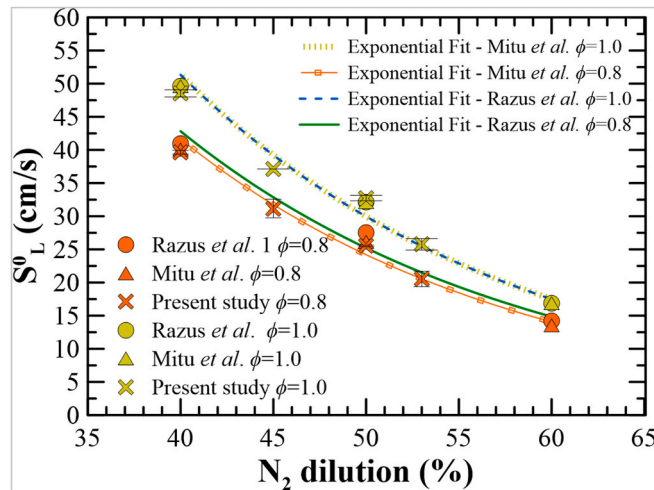


Fig. 4. Experimental laminar burning velocity comparison of CH<sub>4</sub>/N<sub>2</sub>O with 40%–60% N<sub>2</sub> dilution at  $\phi = 0.8, 1.0$ .

formed by combining a sub-mechanism of hydrocarbon chemistry from USC Mech II-2 and a sub-mechanism of nitrogen chemistry from GRI 3.0. In contrast, the US mechanism is formed by combining a sub-mechanism of hydrocarbon chemistry from USC Mech II-2 and a sub-mechanism of nitrogen chemistry from San Diego mechanism. Wang et al. [35] replaced eight UG and US mechanism reactions with different rate constants collected and tested from literature to create UGM and USM mechanisms, respectively. The replaced reactions aim at fixing the rate constants of N<sub>2</sub> and its compounds. Therefore, the rate constants differ among GRI 3.0, USC Mech II-2, and San Diego. Wang et al. [35] compared the aforementioned mechanisms for predicting C<sub>2</sub>H<sub>4</sub>/N<sub>2</sub>O with N<sub>2</sub> dilution under 280 K and 1 atm. They used the two mechanisms to predict and compare the data of CH<sub>4</sub>/N<sub>2</sub>O with N<sub>2</sub> dilution from Powell et al. [15]. In conclusion, the UGM mechanism predicts C<sub>2</sub>H<sub>4</sub>/N<sub>2</sub>O mixtures better, whereas the USM stands out against others in CH<sub>4</sub>/N<sub>2</sub>O mixtures. For validating unstretched laminar burning velocity calculated using the method developed in this study, the ambient temperature and pressure are set to 298 K and 1 atm, respectively.

### 3. Results and discussion

#### 3.1. The laminar burning velocity of CH<sub>4</sub>/air premixed flame

Fig. 2a demonstrates the Schlieren imaging photo with CH<sub>4</sub>/air premixed flame under 50% light blockage. Accordingly, the unstretched laminar burning velocities of CH<sub>4</sub>/air premixed flame ranging from 0.8 to 1.4 were experimentally determined in this study. Combining the experimental results of CH<sub>4</sub>/air premixed flame, the simulation results from Chemkin PRO with GRI 3.0, and recent studies of experimental results, the data are presented in Fig. 2b. The experimental data from Selle et al. [16] (indicated by black dots) are close to the numerical results (indicated by blue line), especially in the fuel-lean region. However, the results of  $\phi = 1.15$  and  $\phi = 1.2$  have more disparity between experimental and numerical data than the fuel-lean region.

The results of Coppens et al. [19] using the heat flux method are indicated by triangles. From  $\phi = 0.8$  to 1.05, the results are slightly lower than the numerical data. High consistent results range from  $\phi = 1.1$  to 1.25. Another set of data using the heat flux method by Bosschaart et al. [37] is indicated by hollow diamonds. The trend of the two datasets using the heat flux method is similar. The results of Bosschaart et al. [37] show better consistency with the numerical data from  $\phi = 1.25$  to 1.35. The data of Halter et al. [38] using a spherical burner is slightly lower than the numerical data and the other studies.

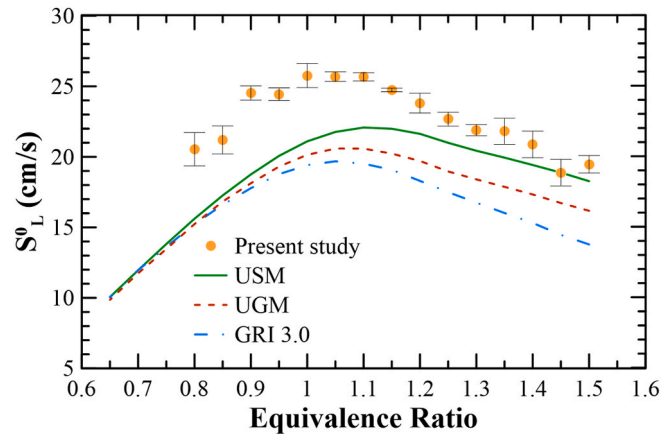


Fig. 5. Experimental ( $\varphi = 0.8$  to  $1.5$ ) and numerical ( $\varphi = 0.65$  to  $1.5$ ) laminar burning velocity of  $\text{CH}_4/\text{N}_2\text{O}$  with 53%  $\text{N}_2$  dilution.

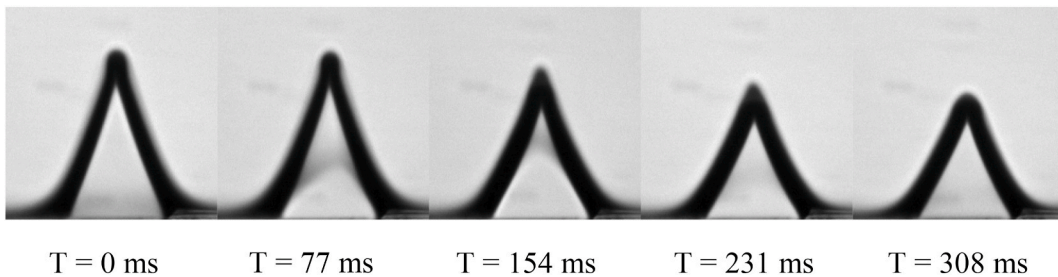


Fig. 6. Schlieren images of  $\text{CH}_4/\text{N}_2\text{O}$  with 53%  $\text{N}_2$  dilution premixed flame at  $\varphi = 1.4$ .

The laminar burning velocities calculated in this present study have a maximum deviation of 13% at  $\varphi = 1.4$  compared with the numerical result. Although the fuel-rich region ( $\varphi = 1.25$  to  $1.4$ ) and  $\varphi = 0.8$  data points have 3.8%–8% disparities, the deviations for  $\varphi = 0.85$  to  $1.2$  are kept below 3.8%. After  $\varphi > 1.3$  region, the flame tip becomes unstable and flickering, especially at  $\varphi = 1.4$ . Fig. 3 displays the Schlieren images of  $\text{CH}_4/\text{air}$  premixed flame at  $\varphi = 1.4$  against time, and it appears the intertwining images at flame tips, leading to measurement uncertainty. Therefore, the suitable measurement equivalence ranges from 0.85 to 1.2.

### 3.2. The laminar burning velocity of $\text{CH}_4/\text{N}_2\text{O}$ with $\text{N}_2$ dilution premixed flame – experimental comparison

In Fig. 4, experimental results from Mitu et al. [39] (indicated by triangles) and Razus et al. [14] (indicated by dots) are acquired using the same methodology. Mitu et al. calculated the laminar burning velocity by assuming the propagation model is adiabatic, whereas Razus et al. assumed it as an isothermal model. In these studies,  $\text{CH}_4/\text{N}_2\text{O}$  mixtures were diluted 40%–60% by  $\text{N}_2$ . The experimental laminar burning velocities calculated in this study include the  $\text{N}_2$  dilution ratio from 40% to 53%. Compared with the adiabatic model by Mitu et al., the average difference is 4.08%. The average difference between the isothermal model by Razus et al. and the present study is 4.55%. Generally, the calculated values of the three datasets are close. At  $\varphi = 0.8$  with 53%  $\text{N}_2$  dilution, the laminar burning velocity reached the lowest value of 20.5 cm/s. The unburned gas supply velocity is 50 cm/s, which is the lowest unburned gas velocity supply limitation. A complete and stable flame front boundary is unable to form for the unburned gas velocity supply, which is below this value. Therefore, the measurement cases for  $>53\%$   $\text{N}_2$  dilution are not presented.

All experimental data show that the laminar burning velocities decrease linearly with an increase in  $\text{N}_2$  dilution for  $\varphi = 0.8$  and  $1.0$ . Furthermore, the velocity differences between  $\varphi = 0.8$  and  $1.0$  are reduced as the  $\text{N}_2$  ratio increases and dominates over the total volume of the mixture. The phenomenon of additive effect on laminar burning velocity is verified by several experimental studies [40] and numerical simulations by Bane et al. [41]. Razus et al. [14] also proposed that the data point with different  $\text{N}_2$  dilutions can be extrapolated between the experimental data points.

### 3.3. Laminar burning velocity of $\text{CH}_4/\text{N}_2\text{O}$ with $\text{N}_2$ dilution premixed flame – experimental and numerical comparison

Experimental laminar burning velocities across  $\varphi = 0.8$  to  $1.5$  are indicated by dots in Fig. 5. The maximum values are found around  $\varphi = 1.0$  to  $1.1$ . At the fuel-lean condition ( $\varphi = 0.8$  and  $0.85$ ) and the fuel-rich condition ( $\varphi = 1.4$  to  $1.5$ ), the data error bars are more significant than other remaining points because of the instability of the flame front boundary. Fig. 6 shows Schlieren images of  $\text{CH}_4/\text{N}_2\text{O}$  with 53%  $\text{N}_2$  dilution premixed flame at  $\varphi = 1.4$  and flow velocity = 80 cm/s. The height of the flame potential cone is various during the time-lapse. This phenomenon was also found in  $\text{CH}_4/\text{air}$  premixed flame at fuel-rich regions ( $\varphi > 1.35$ ) and fuel-lean regions ( $\varphi < 0.9$ ). Additionally, the appropriate unburned gas supply velocities are set from 50 to 80 cm/s for those cases with  $\varphi = 0.9$  to  $1.35$ ,

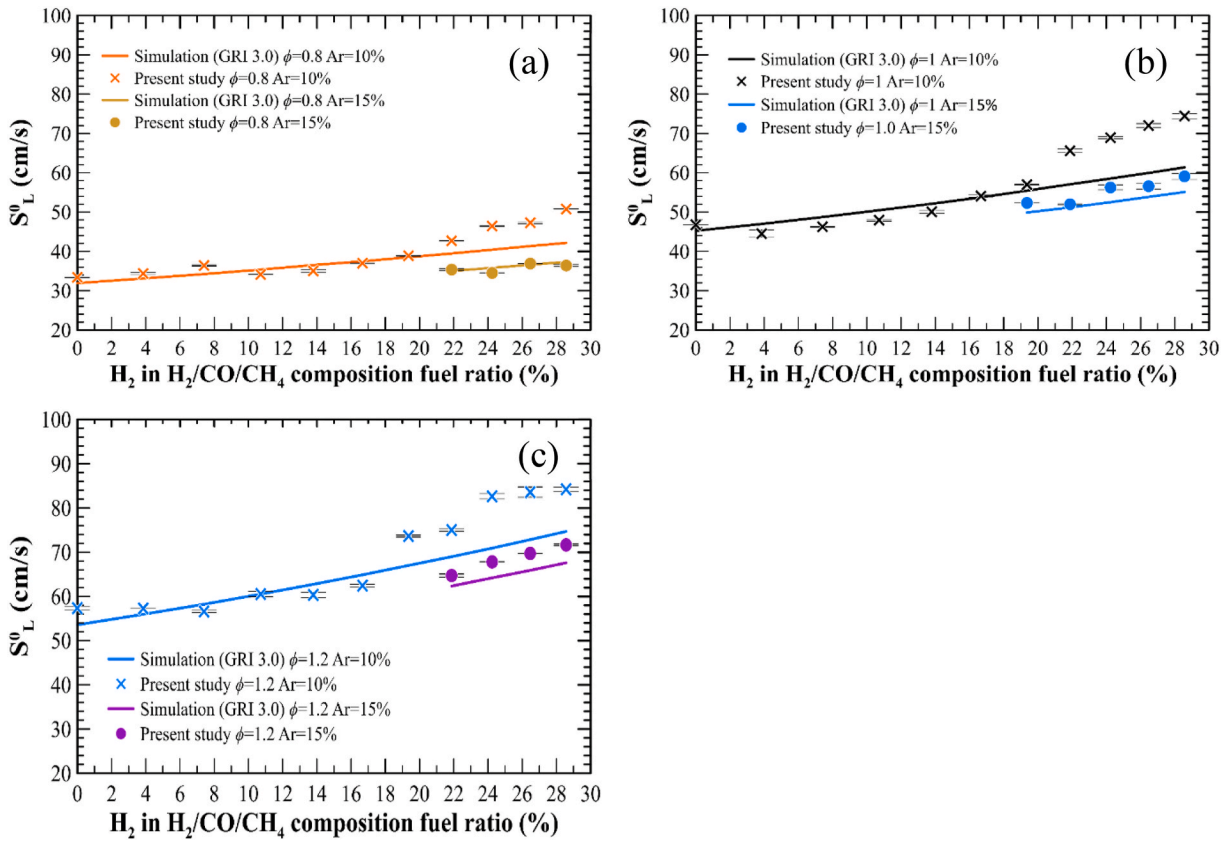


Fig. 7. Laminar burning velocity of syngas with Ar dilution at (a)  $\phi = 0.8$ , (b)  $\phi = 1.0$ , (c)  $\phi = 1.2$ , 0%–28.6%  $H_2$  in fuel ratio.

the data error bars of the unstretched laminar burning velocity of  $CH_4$ /air mixtures are relatively minor in Fig. 5. The unburned gas supply velocities of this region are less than 80 cm/s. However, the jittering, unstable flame front boundary occurred at fuel-rich regions ( $\phi > 1.35$ ) and fuel-lean regions ( $\phi < 0.9$ ) when the unburned gas supply velocity is  $\geq 80$  cm/s or  $\leq 50$  cm/s. It appears that the jittering flame-tip phenomenon is associated with the aerodynamics of the unburned gas mixtures.

Numerical simulation results are presented from  $\phi = 0.65$  to 1.5. The GRI 3.0, UGM, and USM mechanisms are denoted by blue, red, and green lines, respectively. Fig. 5 reveals that the numerical prediction of the laminar burning velocity based on the GRI 3.0 mechanism is apparently low than the experimental results. Similarly, these underestimations in laminar burning velocity were proved in the works of literature [15,35]. The UGM mechanism shows better prediction than GRI 3.0 at stoichiometric and fuel-rich region but is still under predicted. The USM mechanism is proven to have better prediction and tendency for  $CH_4/N_2O$  mixtures by Wang et al. [35], except for data around  $\phi = 1.0$  to 1.2. A similar tendency is also obtained in this study. Numerical results using USM show high consistency with experimental results at the fuel-rich region ( $\phi = 1.25$  and 1.5). However, the difference between the numerical and experimental results in the fuel-lean region becomes more significant.

The differences at the fuel-lean region might be due to relatively high  $N_2O$  concentration. In general,  $N_2O$  is reckoned to be decomposed to nitrogen and oxygen in advance before participating in the chemical reaction. However, in the fuel-lean region, it implies that the oxidizer concentration in the environment is more than required in combustion. Presumably, a partial amount of  $N_2O$  is not decomposed but directly participates in combustion. Yet, the numerical simulation can not predict and embody the role of  $N_2O$  in combustion. Wang et al. [35] also reported that the numerical laminar burning velocities at fuel-lean to stoichiometric are considerably lower than experimental results because of intense chemical reactions in this region. The occurrence of high resemblance at the fuel-rich region is assumed to be related to relatively low  $N_2O$  concentration and low chemical reaction intensity.

### 3.4. The laminar burning velocity of syngas with argon dilution

Experimental and numerical results of laminar burning velocities are shown in Fig. 7.  $H_2$  in fuel ratio increases from 0% to 28.6% at  $\phi = 0.8, 1.0$ , and 1.2. 10 and 15% Argon dilution are mixed in each case. Both experimental (indicated by crosses and dots) and numerical (line) results show that the laminar burning velocity increase with the increase of  $H_2$  concentration in fuel ratio. In numerical results, laminar burning velocities at 0%  $H_2$  are 31.9, 45.2, and 53.6 cm/s for  $\phi = 0.8, 1.0$ , and 1.2, respectively. At 28.6%  $H_2$ , the value rises to 42.2, 61.4, and 74.7 cm/s, indicating that the growth of laminar burning velocity increases with the equivalence ratio and  $H_2$  in fuel ratio. Nevertheless, experimental results share a similar phenomenon.

For the results of  $\phi = 0.8$  (Figs. 7a) and 1.0 (Fig. 7b) with 10% Ar dilution, the differences between experiments and numerical

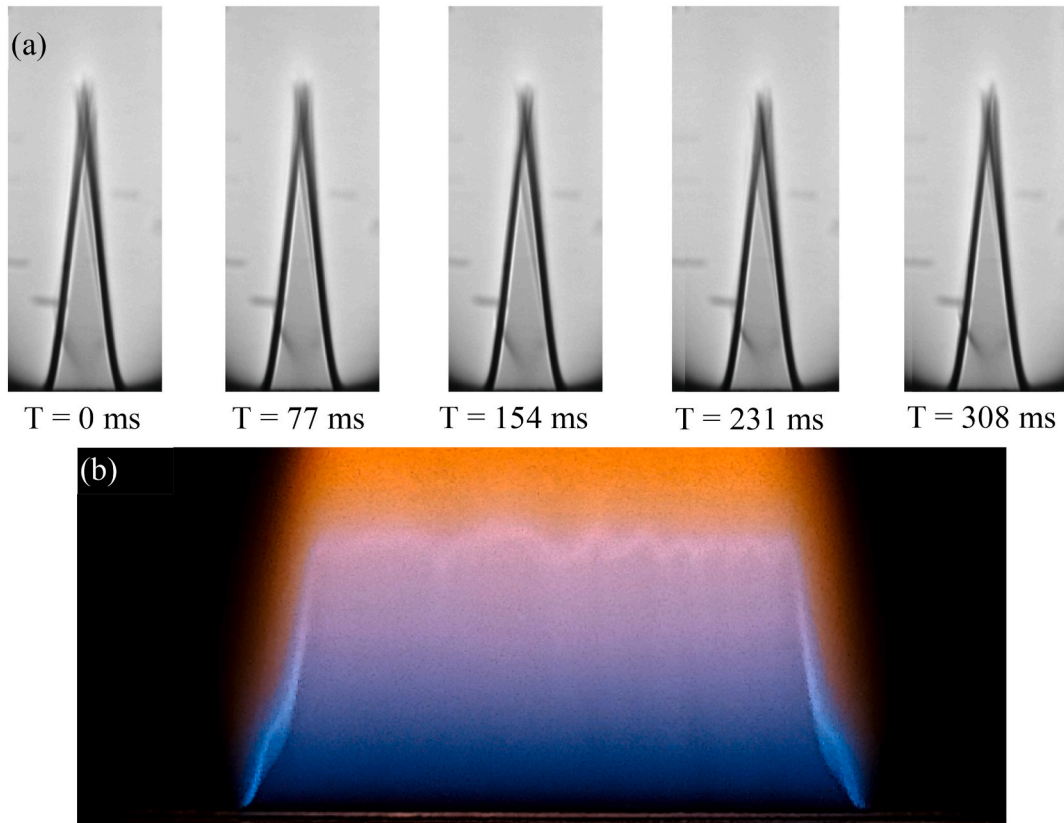


Fig. 8. (a) Schlieren images of syngas at  $\phi = 1.0$  and (b) flame wrinkles.

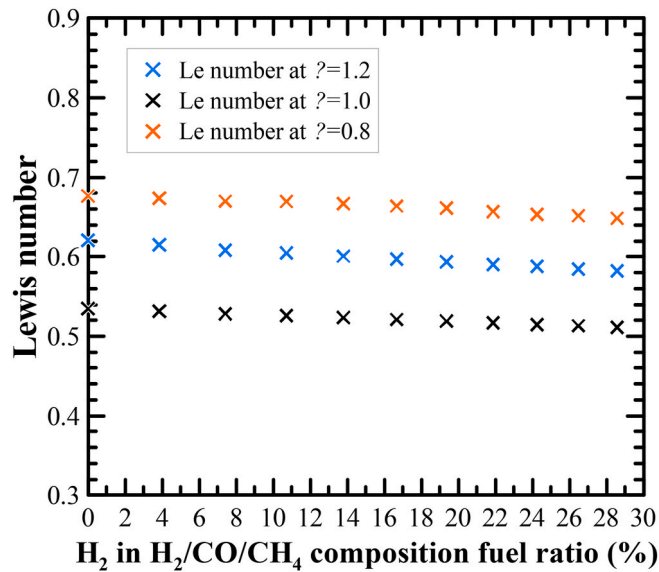


Fig. 9. The Lewis number of syngas with 10% Ar dilution at  $\phi = 0.8, 1.0,$  and  $1.2$ .

simulations are minor until the H<sub>2</sub> ratio reaches 21.9%. Additionally, the instability and wrinkles of the flame happened in this region (Fig. 8), resulting in ambiguous flame front boundaries at the tip. The most significant difference between the numerical and experimental results rises to 21.4% at  $\phi = 1.0$  with 28.6% H<sub>2</sub> mixing ratio. At  $\phi = 1.2$ , the differences rise at 19.4% H<sub>2</sub> with 10% Ar, as shown in Fig. 7c. It is presumed that the differences are related to the H<sub>2</sub> ratio and the corresponding laminar burning velocities and *Le*

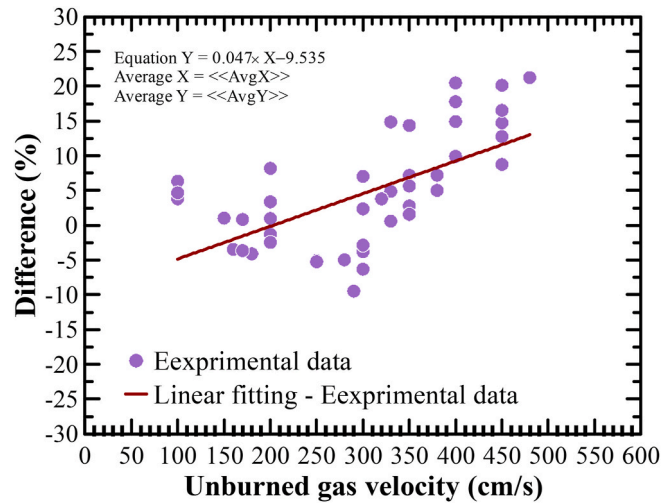


Fig. 10. Correlation of unburned gas velocity and difference of syngas experimental results.

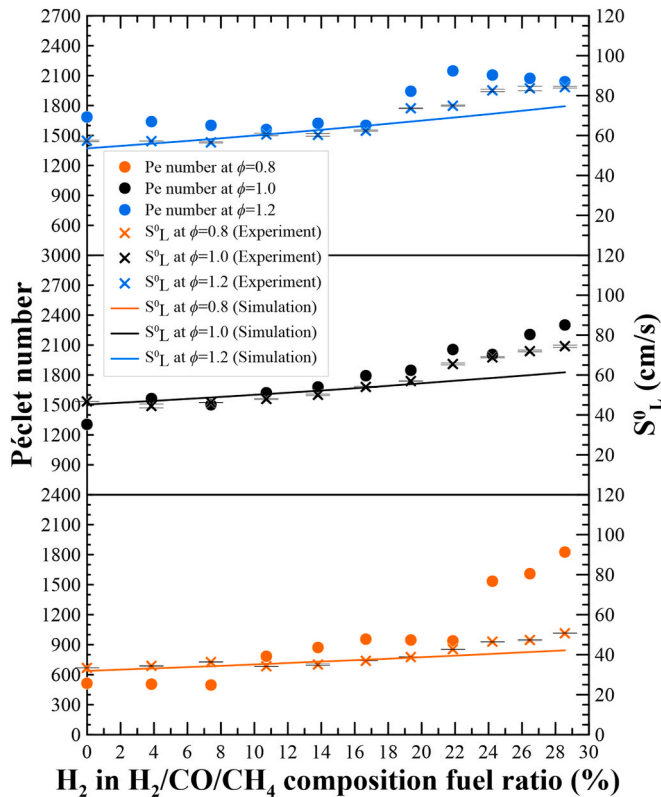


Fig. 11.  $Pe_{pp}$  and laminar burning velocity of syngas with 10% Ar dilution at  $\phi = 0.8, 1.0,$  and  $1.2$ .

(flame front structure is more wrinkled at low  $Le$ ). As shown in Fig. 9, the variation in  $Le$  is minor in each equivalence ratio. To improve the experiment for high  $H_2$  ratio mixtures, more Ar was diluted to decrease laminar burning velocity. As shown in Fig. 7, the differences are significantly decreasing in 15% Ar dilution. The rise in differences is shifted to a higher  $H_2$  ratio.

At  $\phi = 1.2$ , the differences rise at 19.4%  $H_2$  with 10% Ar. After applying the same treatment of 15% Ar dilution in the experiments of  $\phi = 0.8$  and  $1.0$ , the differences also drop. Combining the data of  $\phi = 0.8$  and  $1.0$ , the rise in differences begins once the  $H_2$  ratio reaches 3.67%–3.85% in syngas. Furthermore, the unburned gas supply velocity affects the value of differences, Fig. 10. The linear fitting of Fig. 10 shows the tendency of differences versus the unburned gas velocities. The correlation factor (Pearson correlation coefficient),  $R = 0.61$ , also suggests a positive relationship between the difference in data and unburned gas velocities.

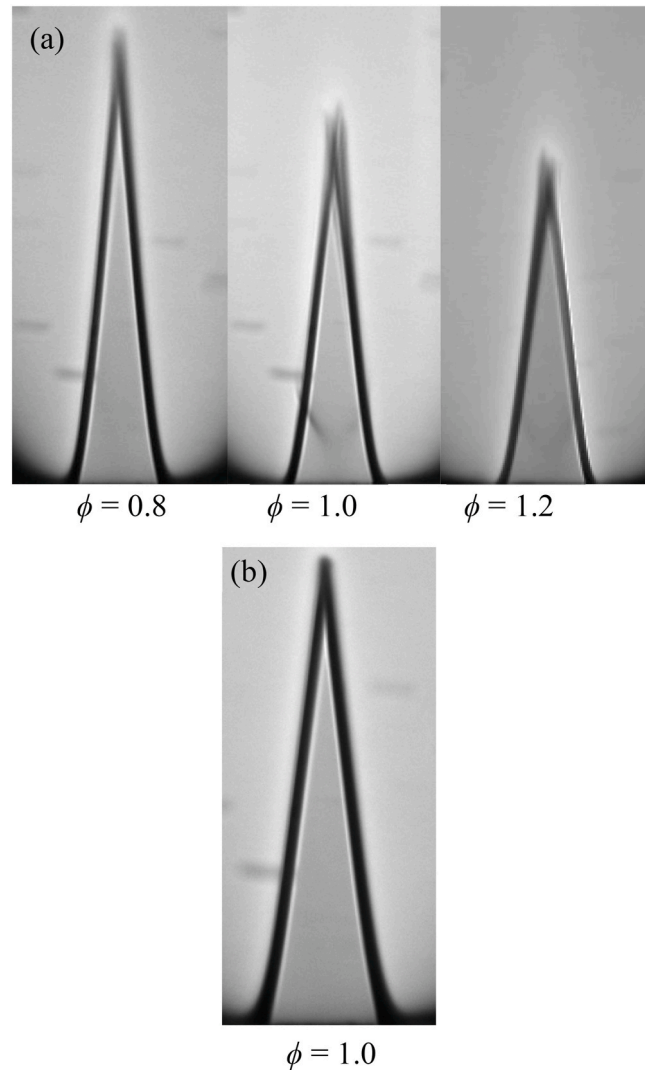


Fig. 12. Schlieren images of (a) syngas at  $\phi = 0.8, 1.0,$  and  $1.2,$  and (b) syngas  $\phi = 1.0$  with 13.8%  $H_2$  in fuel ratio.

**Table 1**  
Recommended parameters' range for aspect ratio of 1:10 slot burner combustion.

$Le$	$Pe_{pr}$	$S_u$	$Re$
$\approx 1.0$	Stable	80–105 cm/s	<1500
0.6–1.0	<1534–1945	80–350 cm/s	<1500
<0.6	<2056	80–350 cm/s	<1500

Fig. 11 shows a comprehensive relationship between differences and  $Pe_{pr}$ . At  $\phi = 0.8$ , the differences in data are minor between  $512 < Pe_{pr} < 938$ . However, significant difference rises at  $Pe_{pr} = 1534$ . At  $\phi = 1.0$ , the difference rises at  $Pe_{pr} = 2056$ . However, the difference rises at  $Pe_{pr} = 1945$ . It is presumed that the threshold of  $Pe_{pr}$  is affected by  $Le$ . Fig. 9 shows that the  $Le$  for  $\phi = 1.0$  is lower than that for  $\phi = 0.8$  and  $1.2$  even though the variation with the  $H_2$  ratio is minor. Therefore, the threshold of  $Pe_{pr}$  increases with the decrease in  $Le$ . It means that the dominant of  $Pr$  or mass diffusion is related to the increase in  $Pe_{pr}$ . The differences in data are also affected by  $Le$ . Chakraborty et al. [7] obtained that flame wrinkle occurs at low  $Le$ . This study shares a similar flame wrinkle, especially at  $\phi = 1.0$  with low  $Le$ . Fig. 12a shows the flame wrinkle at the flame tip with 28.6% of  $H_2$  in fuel. The  $Le$  in Fig. 12a for  $\phi = 0.8, 1.0,$  and  $1.2$  is 0.65, 0.51, and 0.58, respectively.

### 3.5. Instability and difference analyses

For low  $Pe_{pr}$  and low  $Le$  at  $\phi = 1.0$  with 13.8% of  $H_2$  in fuel, the flame front boundary is stable and not wrinkled (Fig. 12b).

**Table 2**  
Influence of parameters in the calculation of laminar burning velocity.

Parameters	Range of influence
$T_b$	0.08%–0.9%
$Le$	0.8%–3.5%
$K$	0.4%–2.2%
$\eta_2$	6.7%
$\delta_L^\circ$	0.9%–2.2%

Generally,  $Pe_{Pr}$  and  $Le$  determine whether the flame front boundary is stable and wrinkled. For  $Le \simeq 1.0$ , which are referred to as  $CH_4$ /air mixtures, the flame front boundaries stay stable and not wrinkled. However, as mentioned in Section 3.2, at  $\varphi = 0.8$  and  $\varphi > 1.35$ , the unstable flame front boundaries are caused by low unburned gas velocity, resulting in larger differences even though  $Le$  is near unity. Some limitations and conditions need to be confirmed to measure laminar burning velocities for more mixtures while using this burner in the future. By collecting the experimental inputs and parameters among  $CH_4$ /air,  $CH_4/N_2O$  with  $N_2$  dilution, and syngas with Ar dilution, the suggested values of the parameters are presented in Table 1.

In calculating the unstretched laminar burning velocity, the flame temperature is related to  $Ze$  and expansion factor,  $\alpha^\circ$ . Manually decreasing the temperature by 50% leads to a 50%  $Ze$  drop and an 80%  $\alpha^\circ$  increase. It seems that the impact of temperature changed significantly affects  $Ze$  and  $\alpha^\circ$ . However, the effect of such modification on the unstretched laminar burning velocity is  $<0.1\%$ . Therefore, in this calculation method, the difference between selecting burned or adiabatic gas temperature as input parameters can be neglected. By modifying the  $Le$  to 1 for syngas, results in a 0.8% difference. This effect increases to 3.5% for cases with low laminar burning velocity. For the stretch rate, 50% modification results in only a 0.4% difference. The correction factor for 2D bulk velocity affects the results by 6.7%, which is the most significant among other parameters. The reason is that  $\eta_2$  is directly connected to the stretch flow field (Table 2). This factor may vary with different aspect ratios of slot burner and the corresponding velocity profile according to the study of Tatsumi et al. [34].

#### 4. ConclusionS

1. In the validation experiment for the provided unstretched laminar burning velocity calculation methodology,  $CH_4$ /air mixtures show decent agreement compared with other studies and GRI 3.0 numerical simulation results at  $\varphi = 0.85$  to 1.2. For fuel-lean and fuel-rich regions, the rise in differences is due to insufficient unburned gas supply velocity. This methodology can provide the unstretched laminar burning velocity at the near stoichiometric region with low differences.
2. The experimental results of  $CH_4/N_2O$  with various  $N_2$  dilution ratios match the data from Razus et al. [14] and Mitu et al. [39]. Comparison between numerical simulation data using GRI 3.0, USM, UGM, and experimental data shows that the best mechanism for predicting the unstretched laminar burning velocity is USM. However, high consistency between the numerical and experimental results only occurs in fuel-rich regions. This study suggests that the prediction using the USM mechanism is reasonable at low  $N_2O$  concentrations.
3. For low  $H_2$  in fuel composition ratio, experimental results match with GRI 3.0 numerical simulation data. As the  $H_2$  ratio increases, instability and wrinkles significantly differ between experimental and numerical simulation data. Thus, the intensity of instability and wrinkles is proportional to the heat transfer Péclet number and inversely proportional to the Lewis number.
4. A flow field with Reynold's number lower than 1500 is recommended for methodology with an aspect ratio of 10:1 slot burner. The effect of temperature on the unstretched laminar burning velocity calculation is minor. The Lewis number influences calculation and cannot be neglected, especially for low laminar burning velocity cases. The importance of the Lewis number is second to the correction factor for the 2D bulk velocity profile. The suggested range of parameters is presented in Table 2. A detailed sensitivity analysis of the calculation process will be completed in the future.
5. Even though this measurement system with a slot burner cannot perform combustion under various pressure and extreme lean or rich mixtures' conditions, it is more convenient and economical than the spherical combustor.

#### Author statement

Yueh-Heng Li: Conceptualization, Supervision, Methodology, Writing- Reviewing and Editing. Jin-Wei Liang: Data Curation, Investigation, Writing- Original draft preparation. Hung-Ju Lin: Software, Validation.

#### Declaration of competing interest

The authors declare that they have no known competing financial interests or personal relationships that could have appeared to influence the work reported in this paper.

#### Acknowledgments

Financial support for this work was provided by the Ministry of Science and Technology (Republic of China, Taiwan) under grant numbers MOST 106-2923-E-006-003-MY3, MOST 108-2628-E-006-008-MY3, and MOST 109-2221-E-006-037-MY3. The authors wish to thank Dr. Guan-Bang Chen for numerical assistance. Computer time and numerical packages provided by the National Center for

High-Performance Computing, Taiwan (NCHC Taiwan), are gratefully acknowledged.

## Appendix A. Supplementary data

Supplementary data to this article can be found online at <https://doi.org/10.1016/j.csite.2022.102162>.

## References

- [1] M. Matalon, On flame stretch, *Combust. Sci. Technol.* 31 (3–4) (1983) 169–181.
- [2] D. Lalpalme, R. Lemaire, P. Seers, Assessment of the method for calculating the Lewis number of H<sub>2</sub>/CO/CH<sub>4</sub> mixtures and comparison with experimental results, *Int. J. Hydrogen Energy* 42 (12) (2017) 8314–8328.
- [3] R. Addabbo, J.K. Bechtold, M. Matalon, Wrinkling of spherically expanding flames, *Proc. Combust. Inst.* 29 (2) (2002) 1527–1535.
- [4] N. Burali, S. Lapointe, B. Bobbitt, G. Blanquart, Y. Xuan, Assessment of the constant non-unity Lewis number assumption in chemically-reacting flows, *Combust. Theor. Model.* 20 (4) (2016) 632–657.
- [5] G. Ozel-Erol, M. Klein, N. Chakraborty, Lewis number effects on flame speed statistics in spherical turbulent premixed flames, *Flow, Turbul. Combust.* 106 (4) (2021) 1043–1063.
- [6] N. Chakraborty, R.S. Cant, Effects of Lewis number on scalar transport in turbulent premixed flames, *Phys. Fluids* 21 (3) (2009), 035110.
- [7] N. Chakraborty, R.S. Cant, Effects of Lewis number on turbulent scalar transport and its modelling in turbulent premixed flames, *Combust. Flame* 156 (7) (2009) 1427–1444.
- [8] E.G. Groff, The cellular nature of confined spherical propane-air flames, *Combust. Flame* 48 (1982) 51–62.
- [9] J. Bechtold, M. Matalon, Hydrodynamic and diffusion effects on the stability of spherically expanding flames, *Combust. Flame* 67 (1) (1987) 77–90.
- [10] D. Bradley, C. Harper, The development of instabilities in laminar explosion flames, *Combust. Flame* 99 (3–4) (1994) 562–572.
- [11] D. Bradley, C.G.W. Sheppard, R. Woolley, D. Greenhalgh, R. Lockett, The development and structure of flame instabilities and cellularity at low Markstein numbers in explosions, *Combust. Flame* 122 (2000) 195–209.
- [12] G. Makhviladze, V. Melikhov, V. Rabinkov, Flame propagation in the channel and flammability limits, *Fire Saf. Sci.* 3 (1991) 875–883.
- [13] A.N. Mazas, B. Fiorina, D.A. Lacoste, T. Schuller, Effects of water vapor addition on the laminar burning velocity of oxygen-enriched methane flames, *Combust. Flame* 158 (12) (2011) 2428–2440.
- [14] D. Razus, M. Mitu, V. Giurcan, C. Movileanu, D. Oancea, Methane-unconventional oxidant flames. Laminar burning velocities of nitrogen-diluted methane–N<sub>2</sub>O mixtures, *Process Saf. Environ. Protect.* 114 (2018) 240–250.
- [15] O.A. Powell, P. Papas, C. Dreyer, Laminar burning velocities for hydrogen-, methane-, acetylene-, and propane-nitrous oxide flames, *Combust. Sci. Technol.* 181 (7) (2009) 917–936.
- [16] L. Selle, T. Poinso, B. Ferret, Experimental and numerical study of the accuracy of flame-speed measurements for methane/air combustion in a slot burner, *Combust. Flame* 158 (1) (2011) 146–154.
- [17] C.T. Chong, S. Hochgreb, Measurements of laminar flame speeds of liquid fuels: Jet-A1, diesel, palm methyl esters and blends using particle imaging velocimetry (PIV), *Proc. Combust. Inst.* 33 (1) (2011) 979–986.
- [18] S. Wang, Z. Wang, Y. He, X. Han, Z. Sun, Y. Zhu, et al., Laminar burning velocities of CH<sub>4</sub>/O<sub>2</sub>/N<sub>2</sub> and oxygen-enriched CH<sub>4</sub>/O<sub>2</sub>/CO<sub>2</sub> flames at elevated pressures measured using the heat flux method, *Fuel* 259 (2020), 116152.
- [19] F.H.V. Coppens, J. De Ruyck, A.A. Konnov, Effects of hydrogen enrichment on adiabatic burning velocity and NO formation in methane+air flames, *Exp. Therm. Fluid Sci.* 31 (5) (2007) 437–444.
- [20] T. Faravelli Af, E. Ranzi, Kinetic modeling of the interactions between NO and hydrocarbons in the oxidation of hydrocarbons at low temperatures, *Combust. Flame* 132 (2003) 188–207.
- [21] S. Parres-Esclapez, M.J. Illán-Gómez, C.S.-M. de Lecea, A. Bueno-López, On the importance of the catalyst redox properties in the N<sub>2</sub>O decomposition over alumina and ceria supported Rh, Pd and Pt, *Appl. Catal. B Environ.* 96 (3–4) (2010) 370–378.
- [22] W.-L. Chen, C.-W. Huang, Y.-H. Li, C.-C. Kao, H.T. Cong, Biosyngas-fueled platinum reactor applied in micro combined heat and power system with a thermophotovoltaic array and stirling engine, *Energy* 194 (2020), 116862.
- [23] Y.-H. Li, H.-H. Chen, Analysis of syngas production rate in empty fruit bunch steam gasification with varying control factors, *Int. J. Hydrogen Energy* 43 (2) (2018) 667–675.
- [24] Y.-H. Li, H.-W. Hsu, Y.-S. Lien, Y.-C. Chao, Design of a novel hydrogen–syngas catalytic mesh combustor, *Int. J. Hydrogen Energy* 34 (19) (2009) 8322–8328.
- [25] C.-H. Chen, Y.-H. Li, Role of N<sub>2</sub>O and equivalence ratio on NO<sub>x</sub> formation of methane/nitrous oxide premixed flames, *Combust. Flame* 223 (2021) 42–54.
- [26] Y.-H. Li, C.-H. Chen, M. Ilbas, Effect of diluent addition on combustion characteristics of methane/nitrous oxide inverse Tri-Coflow diffusion flames, *Combust. Sci. Technol.* (2020) 1–21.
- [27] Y.-H. Li, S.K. Reddy, C.-H. Chen, Effects of the nitrous oxide decomposition reaction on soot precursors in nitrous oxide/ethylene diffusion flames, *Energy* 235 (2021), 121364.
- [28] A.A. Konnov, I.V. Dyakov, Nitrous oxide conversion in laminar premixed flames of CH<sub>4</sub>+O<sub>2</sub>+Ar, *Proc. Combust. Inst.* 32 (1) (2009) 319–326.
- [29] T. Scholte, P. Vaags, Burning velocities of mixtures of hydrogen, carbon monoxide and methane with air, *Combust. Flame* 3 (1959) 511–524.
- [30] M. Cherian, P. Rhodes, R. Simpson, G. Dixon-Lewis, Structure, chemical mechanism and properties of premixed flames in mixtures of carbon monoxide, nitrogen and oxygen with hydrogen and water vapour, *Phil. Trans. Roy. Soc. Lond. Math. Phys. Sci.* 303 (1476) (1981) 181–212.
- [31] C.J. Rallis, A.M. Garforth, The determination of laminar burning velocity, *Prog. Energy Combust. Sci.* 6 (4) (1980) 303–329.
- [32] D. Bunjong, N. Pussadee, P. Wattanakaswich, Optimized conditions of Schlieren photography, *J. Phys. Conf.* 1144 (2018), 012097.
- [33] K.T. Walsh, J. Fielding, M.B. Long, Effect of light-collection geometry on reconstruction errors in Abel inversions, *Opt. Lett.* 25 (7) (2000) 457–459.
- [34] T. Tatsumi, T. Yoshimura, Stability of the laminar flow in a rectangular duct, *J. Fluid Mech.* 212 (1990) 437–449.
- [35] W. Wang, H. Zhang, Laminar burning velocities of C<sub>2</sub>H<sub>4</sub>/N<sub>2</sub>O flames: experimental study and its chemical kinetics mechanism, *Combust. Flame* 202 (2019) 362–375.
- [36] Y. Wang, A. Movaghar, Z. Wang, Z. Liu, W. Sun, F.N. Egolopoulos, et al., Laminar flame speeds of methane/air mixtures at engine conditions: performance of different kinetic models and power-law correlations, *Combust. Flame* 218 (2020) 101–108.
- [37] K.J. Bosschaart, L.P.H. de Goeij, Detailed analysis of the heat flux method for measuring burning velocities, *Combust. Flame* 132 (1) (2003) 170–180.
- [38] F. Halter, C. Chauveau, N. Djebaïli-Chaumeix, I. Gökalp, Characterization of the effects of pressure and hydrogen concentration on laminar burning velocities of methane–hydrogen–air mixtures, *Proc. Combust. Inst.* 30 (1) (2005) 201–208.
- [39] M. Mitu, V. Giurcan, C. Movileanu, D. Razus, D. Oancea, Propagation of CH<sub>4</sub>-N<sub>2</sub>O-N<sub>2</sub> flames in a closed spherical vessel, *Processes* 9 (2021) 851.
- [40] M. Mitu, V. Giurcan, D. Razus, D. Oancea, Inert gas influence on the laminar burning velocity of methane–air mixtures, *J. Hazard Mater.* 321 (2017) 440–448.
- [41] S.P.M. Bane, R. Mével, S.A. Coronel, J.E. Shepherd, Flame burning speeds and combustion characteristics of undiluted and nitrogen-diluted hydrogen–nitrous oxide mixtures, *Int. J. Hydrogen Energy* 36 (16) (2011) 10107–10116.
- [42] Yueh-Heng Li, Guan-Bang Chen, Yi-Chieh Lin, Yei-Chin Chao, Effects of flue gas recirculation on the premixed oxy-methane flames in atmospheric condition, *Energy* 89 (2015) 845–857, <https://doi.org/10.1016/j.energy.2015.06.032>. In this issue.